Detecting Chemical Hazards with Temperature-Programmed Microsensors: Overcoming Complex Analytical Problems with Multidimensional Databases*

Douglas C. Meier, Baranidharan Raman, and Steve Semancik

Chemical Science and Technology Laboratory, National Institute of Standards and Technology, Gaithersburg, Maryland 20899-8362; email: dmeier@nist.gov, braman@nist.gov, steves@nist.gov

Key Words

chemiresistive, gas sensor, microarray, temperature dependence, toxic industrial chemicals, pattern recognition

Abstract

Complex analytical problems, such as detecting trace quantities of hazardous chemicals in challenging environments, require solutions that most effectively extract relevant information about a sample's composition. This review presents a chemiresistive microarray–based approach to identifying targets that combines temperature-programmed elements capable of rapidly generating analytically rich data sets with statistical pattern recognition algorithms for extracting multivariate chemical fingerprints. We describe the chemical-microsensor platform and discuss its ability to generate orthogonal data through materials selection and temperature programming. Visual inspection of data sets reveals device selectivity, but statistical analyses are required to perform more complex identification tasks. Finally, we discuss recent advances in both devices and algorithms necessary to deal with practical issues involved in long-term deployment. These issues include identification and correction of signal drift, challenges surrounding real-time unsupervised operation, repeatable device manufacturability, and hierarchical classification schemes designed to deduce the chemical composition of untrained analyte species.

1. INTRODUCTION

The difficulties associated with detecting chemical hazards are myriad. Hazardous molecules span a wide range of sizes, from toxic industrial chemicals (TICs) such as HCN (three atoms, formula weight 27) to chemical warfare agents (CWAs) such as VX nerve agent (42 atoms, formula weight 267) and beyond. Hazardous compounds also include a variety of functional groups, such as the organic phosphonate nerve agents, the halogenated thioether and alkylamine blister agents, and the nitrile blood agents. The detection device must therefore possess the flexibility to measure a range of diverse chemicals to provide broad-spectrum threat protection. The variety of background conditions and the potential presence of other benign compounds further exacerbate the problem because the detection system must be both selective for molecular threats and sensitive to them. The requirements of protective detection present additional challenges. Because the chosen analytical tool is intended to prevent harm due to poisonous chemicals, sensitivity to these compounds must be amplified to cover subhazardous concentrations. Rapid detection is also a priority, as threats rapidly identified must be readily located and countered to prevent further injury. Finally, a detection system capable of meeting all of these challenges must be widely deployable at an acceptable cost to be truly practical for perimeter security and wide-area protection.

Figure 1 schematically represents a realistic example of the challenging background environments that could be faced by a hazardous-chemical detection system on a given day. The detector comes into contact with one of several hazardous analytes at the IDLH (immediate danger to life and health) concentration 10 times in as many hours. The relative humidity ranges from 10% to 70%. Periodically, the fumes from one of four different household products (floor stripper, paint, bleach, and window cleaner, all at 1% of their saturation vapor pressures) are introduced to the detector. When the individual cycles for five different target compounds are complete, the detector system has been presented with 42 different combinations of analyte and background, not including possible history effects upon the device.

Problems of such complexity require both advanced instruments and advanced operational algorithms, or higher-order sensing (1), to surmount the challenges of sensitivity, selectivity, speed, and deployability. **Figure 2** illustrates methods (discussed below) to manipulate the available coding space of an analytical instrument to meet the demand posed by the chemical-detection task. Although zero-dimensional (0-D; **Figure 2a**) and one-dimensional (1-D; **Figure 2b**) measurements may be appropriate for simpler problems, higher-dimensional approaches (2-D and beyond; **Figure 2c,d**) are required for tasks similar to those described in **Figure 1**. To rapidly generate vast multidimensional databases, we exploit the favorable properties of a chemical-microsensor platform based on microelectromechanical systems (MEMS).

2. MICROELECTROMECHANICAL SYSTEMS–BASED CHEMICAL MICROARRAY TECHNOLOGY

2.1. The Microsensor Device

The microhotplate array platform has been central to our chemical sensor research (2–4). The scanning electron micrograph image shown in **Figure 3a** and the exploded schematic in **Figure 3b** illustrate the most useful features of a single sensor element within the array. The device elements are small (with lateral dimensions on the order of 100 μm), include doped polycrystalline silicon resistors sandwiched between layers of silicon oxide, and are topped with patterned electrodes. When wet chemical micromachining etches away the silicon underlying a microhotplate element, it is released from the substrate. The buried resistor then behaves as a fast heater, with millisecond
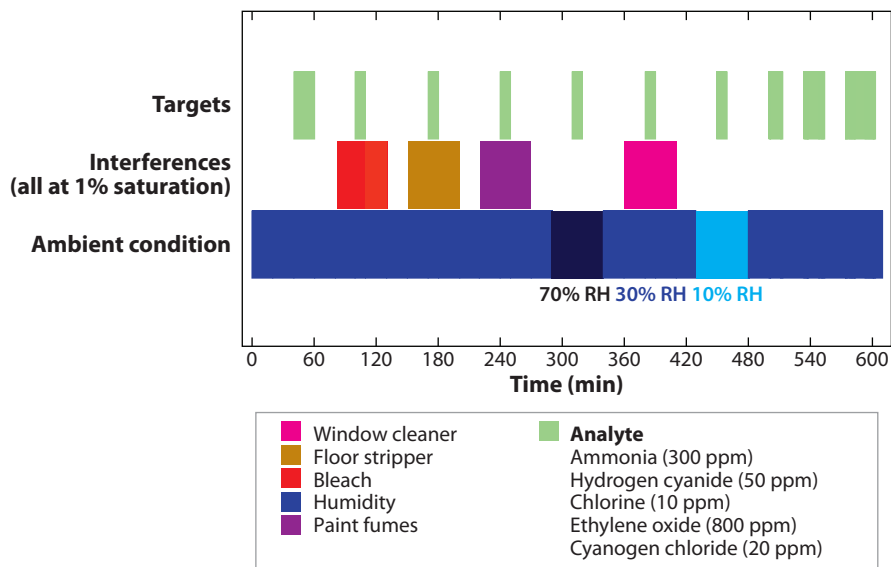
Figure 1

The target analyte (and background) delivery sequence used during the chemical microsensor studies, which attempts to capture the complexity of real-world detection problems such as humidity changes and the introduction of relatively high concentrations of common household products.

response times and an operating temperature range from ambient to 500° C. This design makes the microhotplate an excellent platform for deposition and processing of materials on the microscale (5). This MEMS device element can be readily duplicated on a silicon wafer to form arrays (such as the 16-element array shown in **Figure 3c**), in which each element can be operated independently of the others. This feature allows for different thermally and electrically activated materials-deposition processes to be performed on individual elements within an array, resulting in arrays whose separate elements can be easily populated with different sensitive materials. Finally, thousands of these arrays can be built on a 6-inch-diameter silicon wafer, promising mass manufacturability and the concomitant cost savings that arise from increasing returns to scale. Sensor devices for work included in this review were produced from arrays designed at the National Institute of Standards and Technology (NIST), produced in wafer runs at MIT Lincoln Laboratory,[1] and micromachined at NIST. A fully functional array wire-bonded into a 40-pin dual-inline package is shown in **Figure 3d**.

Our research team and collaborators have exploited the microscale materials–processing aspect of microsensor technology to produce a large, varied materials toolbox for maximum coverage of different target analytes and application spaces. A selection of some of the conductometric sensing materials successfully used with the microhotplate arrays is shown in **Figure 4** (6). These materials include a nanostructured semiconducting metal oxide film deposited by thermally activated single-source chemical vapor deposition (CVD; **Figure 4a**). Films deposited using this method include tin oxide (SnO_2), titanium oxide (TiO_2), alternating layers of these metal oxides

---

[1]The full description of the procedures used in this paper requires the identification of certain commercial products and their suppliers. The inclusion of such information should in no way be construed as indicating that such products or suppliers are endorsed by NIST or are recommended by NIST or that they are necessarily the best materials, instruments, software, or suppliers for the purposes described.

(TiO$_2$/SnO$_2$), and ruthenium-coated titanium oxide (Ru/TiO$_2$). A variety of source materials, deposition temperatures and times, and preprocessing and postprocessing procedures have been utilized to deposit electrically conductive oxide films, and many of these materials have successfully produced sensitive films for analyte measurement (6–8). The sensing principle for such films is essentially analogous to that of the Taguchi sensor (9), a conductometric device that measures the
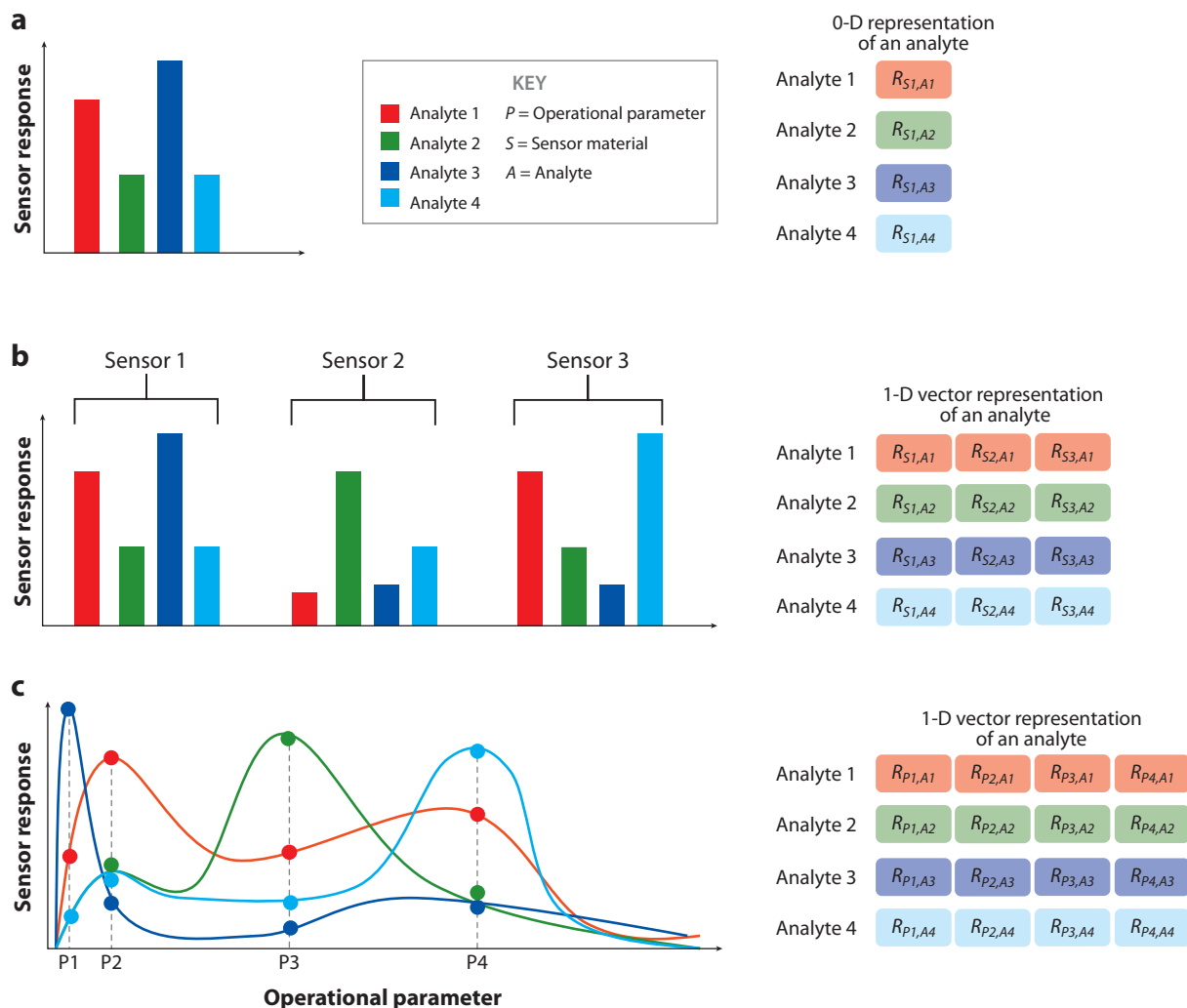

Figure 2

Possible approach to confronting analytical challenges of the kind illustrated in **Figure 1**. (*a*) A zero-dimensional (0-D) approach. The response of a single sensor measured with fixed operating parameters (e.g., temperature, flow rate) constitutes a set of 0-D points for each analyte, whose value changes as a function of analyte identity and intensity. Discrimination is achieved by comparing these real-valued responses. (*b*, *c*) One-dimensional (1-D) approaches. Measurements either from multiple sensors with fixed operating parameters or from a single sensor with systematically modulated operation parameters yield a 1-D response vector for each analyte that becomes the chemical fingerprint. (*d*) A two-dimensional (2-D) approach. Capturing responses of multiple materials at different operating parameter values yields a 2-D response matrix for each analyte, from which the chemical fingerprint must be extracted. (*e*) Higher-dimensional approaches. Capturing the response of multiple sensors by modulating one or more operation parameter(s) and/or their dynamics over time results in high-dimensional data structures that contain the analyte's chemical signature.
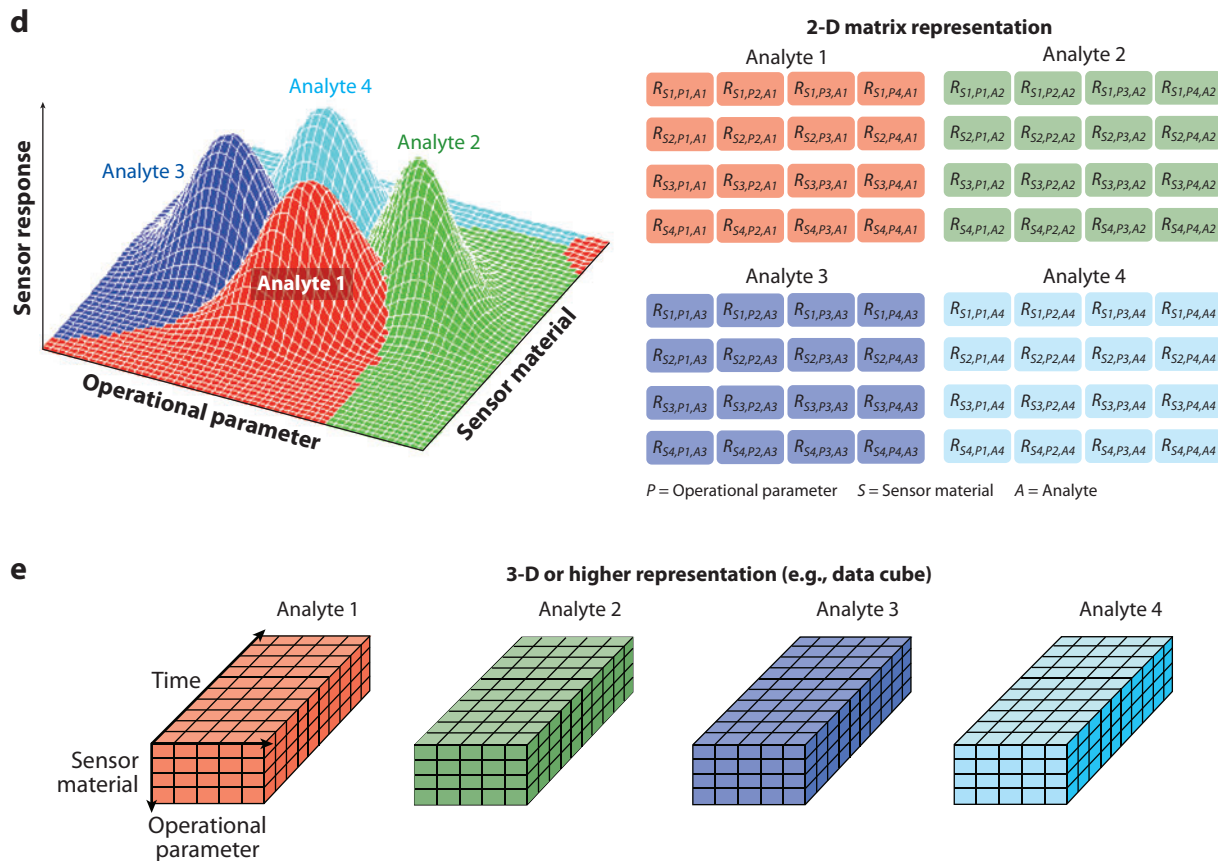
d

2-D matrix representation

Analyte 1

$R_{S1,P1,A1}$ $R_{S1,P2,A1}$ $R_{S1,P3,A1}$ $R_{S1,P4,A1}$

$R_{S2,P1,A1}$ $R_{S2,P2,A1}$ $R_{S2,P3,A1}$ $R_{S2,P4,A1}$

$R_{S3,P1,A1}$ $R_{S3,P2,A1}$ $R_{S3,P3,A1}$ $R_{S3,P4,A1}$

$R_{S4,P1,A1}$ $R_{S4,P2,A1}$ $R_{S4,P3,A1}$ $R_{S4,P4,A1}$

Analyte 2

$R_{S1,P1,A2}$ $R_{S1,P2,A2}$ $R_{S1,P3,A2}$ $R_{S1,P4,A2}$

$R_{S2,P1,A2}$ $R_{S2,P2,A2}$ $R_{S2,P3,A2}$ $R_{S2,P4,A2}$

$R_{S3,P1,A2}$ $R_{S3,P2,A2}$ $R_{S3,P3,A2}$ $R_{S3,P4,A2}$

$R_{S4,P1,A2}$ $R_{S4,P2,A2}$ $R_{S4,P3,A2}$ $R_{S4,P4,A2}$

Analyte 3

$R_{S1,P1,A3}$ $R_{S1,P2,A3}$ $R_{S1,P3,A3}$ $R_{S1,P4,A3}$

$R_{S2,P1,A3}$ $R_{S2,P2,A3}$ $R_{S2,P3,A3}$ $R_{S2,P4,A3}$

$R_{S3,P1,A3}$ $R_{S3,P2,A3}$ $R_{S3,P3,A3}$ $R_{S3,P4,A3}$

$R_{S4,P1,A3}$ $R_{S4,P2,A3}$ $R_{S4,P3,A3}$ $R_{S4,P4,A3}$

Analyte 4

$R_{S1,P1,A4}$ $R_{S1,P2,A4}$ $R_{S1,P3,A4}$ $R_{S1,P4,A4}$

$R_{S2,P1,A4}$ $R_{S2,P2,A4}$ $R_{S2,P3,A4}$ $R_{S2,P4,A4}$

$R_{S3,P1,A4}$ $R_{S3,P2,A4}$ $R_{S3,P3,A4}$ $R_{S3,P4,A4}$

$R_{S4,P1,A4}$ $R_{S4,P2,A4}$ $R_{S4,P3,A4}$ $R_{S4,P4,A4}$

P = Operational parameter S = Sensor material A = Analyte

e

3-D or higher representation (e.g., data cube)

Analyte 1   Analyte 2   Analyte 3   Analyte 4

Time

Sensor material

Operational parameter

Figure 2

Continued

concentration of reducing gases in contact with a macroscopic tin oxide gel by monitoring the oxide's electrical conductance. **Figure 4b** shows a sintered mesoporous TiO_2 sensing film that operates largely as CVD TiO_2 films do but that is applied from solution rather than from vapor. One can readily tailor the morphology of solution-deposited films by, for instance, depositing polymer microspheres coated with the sensing material, then sintering to remove the labile polymer, leaving the shell with a greatly enhanced surface area–to–bulk volume ratio and a higher sensitivity. An example of antimony-doped SnO_2 microspheres assembled from 1.5-nm particles is shown in **Figure 4c** (10). Conductive chemically sensitive polymers such as polyaniline can also be deposited on the microsensor (**Figure 4d**); the structure, morphology, and chemical-sensing properties of the electroactive polymer can be adjusted electrochemically and by altering pH (11), thereby tuning the sensor response. Other sensing materials successfully deployed include carbon-loaded polymers (12), metal nanoparticle–seeded metal oxides (13), and single SnO_2 nanowires (14).

2.2. Fixed-Temperature Sensing

Once a conductive, chemically sensitive film is applied to electrically bridge the top contacts of the sensor device, sensing is performed by measuring the electrical conductance of the film
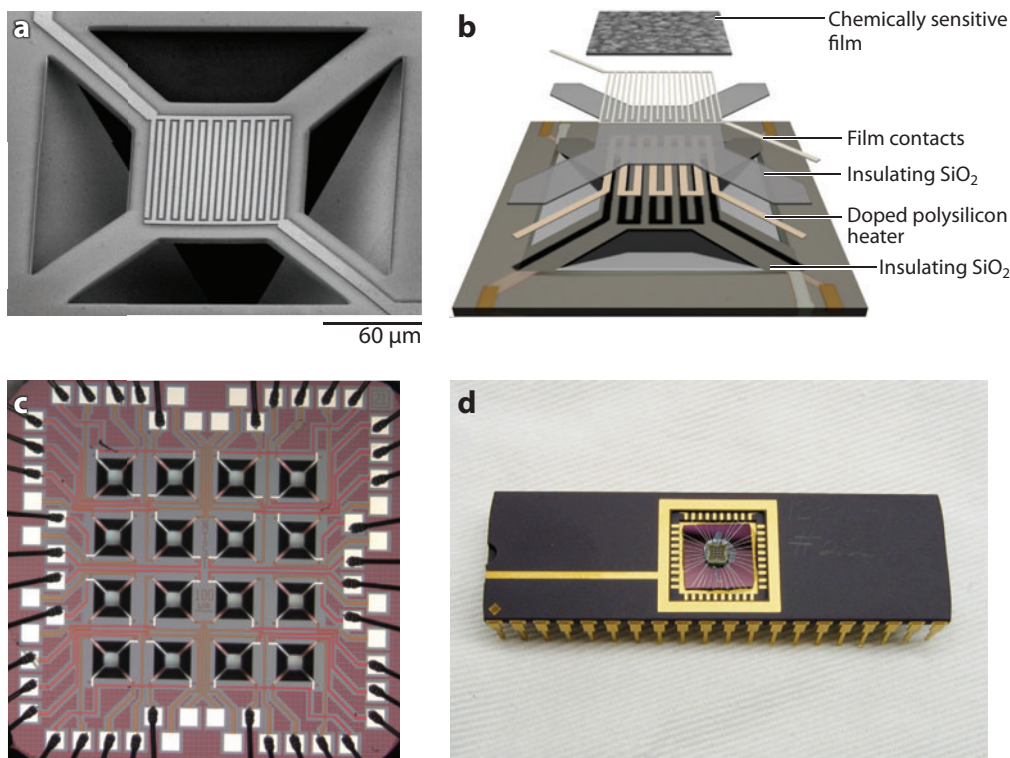
a

60 μm

b

Chemically sensitive
film

Film contacts

Insulating SiO_2

Doped polysilicon
heater

Insulating SiO_2

c

d

Figure 3

(*a*) Top view of a single chemical-sensor element. (*b*) Expanded schematic of the critical components of the microsensor device.
(*c*) A 16-element microsensor array. (*d*) A sensor array packaged and wire-bonded into a 40-pin dual-inline package.

while exposing it to chemical environments of interest. If the film is maintained at constant temperature, a conductance change measured during a given condition change confirms sensitivity. This operating mode of the microsensor is referred to as fixed-temperature sensing (FTS). It is the mode we have used to confirm film sensitivity to analytes and to assess signal as a function of concentration (i.e., dynamic range). This mode has been frequently used in prior exploratory studies designed to characterize both materials and analyte responses as well as cross-talk between sensing elements in the same array (13, 15). **Figure 5** (16) shows an example of an FTS plot for two sensors (one SnO_2, the other TiO_2) exposed to the nerve agent GB (sarin) at a series of concentrations. This simple experiment shows that both the highly resistive TiO_2 and the more conductive SnO_2 are sensitive to sublethal concentrations of sarin [the 30-min median lethal concentration of GB is 800 nmol mol^{-1} (17)]. However, the sensors also exhibit differing dynamic ranges with respect to GB detection. Whereas SnO_2 provides a roughly linear response with concentration at every temperature tested, only at the highest operating temperature does TiO_2 provide concentration-dependent information. This device was also used in FTS mode to successfully detect the blister agent HD (sulfur mustard) and the nerve agent GA (tabun) at sublethal concentrations (16, 18). In addition to the sensor's ability to gauge baseline sensitivity and dynamic range, the investigators observed that the sensitive materials at the explored operating temperatures exhibit characteristic signal-onset and recovery times (on the order of seconds) upon target-analyte introduction and removal. These results suggest that the data contain information
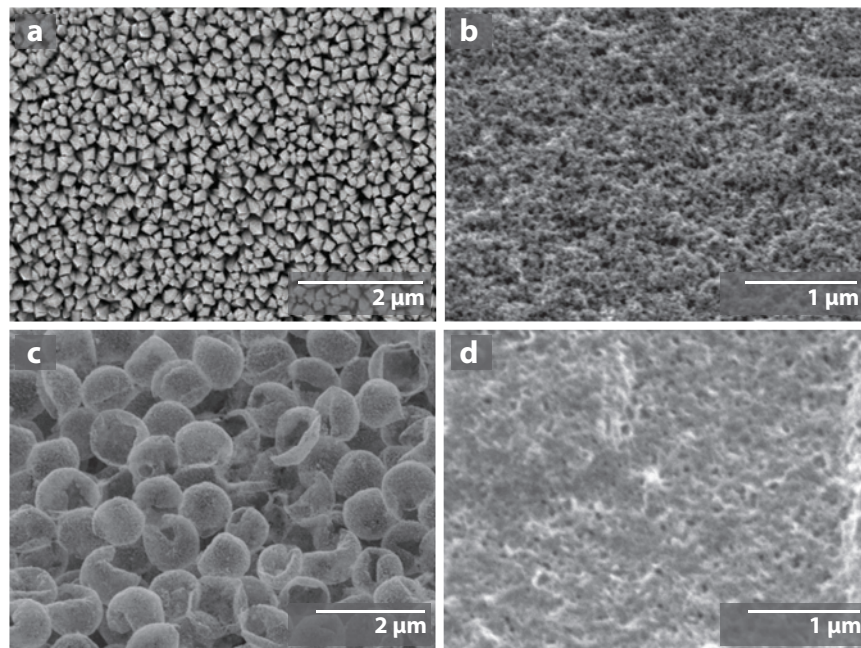
Figure 4

Scanning electron microscope images of a variety of chemically sensitive films deposited on microhotplate-sensor platforms. (*a*) Polycrystalline metal oxide films deposited via chemical vapor deposition. Shown here is tin oxide (SnO_2); titanium oxide (TiO_2), TiO_2 layered on SnO_2, and ruthenium (Ru) deposited on TiO_2 have also been used. (*b*) Mesoporous TiO_2 film applied by drop coating. (*c*) Drop-coated shells of $Sb:SnO_2$. (*d*) Electrophoretically deposited nanostructured conductive polymer (here, colloidal polyaniline). Images are shown at different scales to highlight each film's nanostructure and morphology.

on short-term gas–surface interactions and could therefore be cycled more rapidly through the available temperature range to generate more information.

2.3. Temperature-Programmed Sensing

Although FTS is useful for determining many characteristics of a sensor's interaction with a chemical environment, it operates as a 0-D analytical tool on short timescales, providing only a single conductance value for a single sensing material (analogous to the output of a thermometer). Many analytes, regardless of their degree of lethality, exhibit reductive (increasing conductance) or oxidative (decreasing conductance) interactions with metal oxide sensing films. For example, SnO_2 nanoparticle films have been shown to detect methanol in air at concentrations as low as 10 ppb (19). This selectivity problem may be further complicated by the presence of other vapors (such as water) in a hazardous gas mixture, thereby changing the single-valued signal generated by a single sensor at constant temperature.

Chemical sensing can benefit from variable-temperature signal generation. We note that response sensitivities have been correlated to temperature for a variety of sensing materials and target analytes (e.g., 20, 21). Thermal gradients have also been applied to a (macroscopic) sensing material while conductance measurements are made at intervals along the gradient in order to use the relative analyte sensitivities with temperature as a discrimination function (22, 23). In addition,
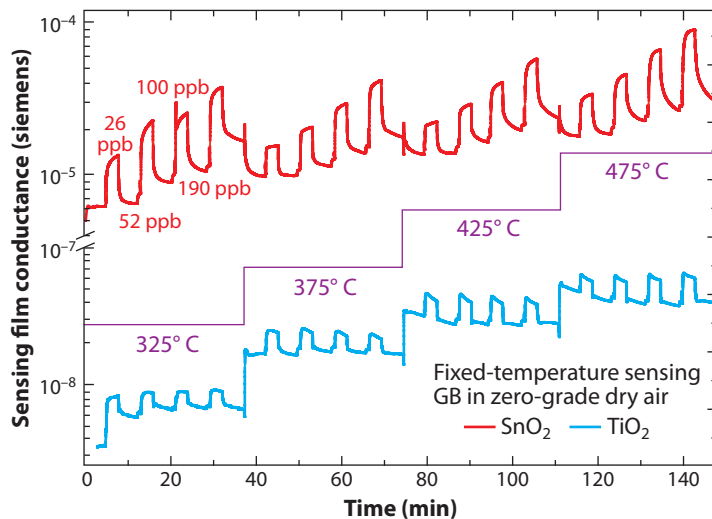
Figure 5

Fixed-temperature sensing signal from a sensor array, including SnO_2 and TiO_2 sensing films, upon
exposure to GB (sarin) in concentrations from 26 nmol mol^{-1} (ppb) to 190 ppb in zero-grade dry air. The
analyte was introduced under continuous flow, and the program was repeated at sensor temperatures from
325° C to 475° C in 50°-C increments.

other researchers have studied temperature modulation applied at a relatively low frequency to a
single (commercial) sensor. They report a somewhat expanded information stream that permits
identification of a larger range of analytes with such a device (24, 25, 26). The approach reviewed
herein relies on low-power, temperature-pulsed microdevices and utilizes rapid (~100-ms duty cy-
cle) temperature programming to collect data of high temporal information density to characterize
complex gas-phase streams. The remainder of this review focuses specifically on the acquisition
and processing of these multidimensional databases.

By using the microsensor's high-speed temperature-control capability and by taking advan-
tage of the time-dependent component of the sensing film's response to a given target ana-
lyte, significantly more information about a chemical system can be obtained, which may give
rise to enhanced selectivity. The operational technique used to perform this function is termed
temperature-programmed sensing (TPS). This powerful technique was first used to separate the
signals of volatile organic compounds in air (4, 27, 28). More recently, we used it to identify CWAs
(7, 16, 18) and TICs (7) under a variety of background conditions (as discussed below).

A TPS program is shown in **Figure 6**. When operated by this method, a single NIST mi-
crosensor can sample tens of temperatures in seconds and can treat each data point as a separate,
virtual sensor. In essence, our 0-D data generator becomes a 1-D generator (analogous to, for
example, an infrared spectrometer) through the application of TPS. Adding more sensors fea-
turing different films introduces a material dimension; thus, a 2-D data generator (analogous to
gas chromatography–mass spectrometry techniques) emerges. When the data are viewed in order
of temporal collection, a repeatable pattern emerges. These patterns change when analytes are
introduced; the changes are distinguishable when they are overlaid. **Figure 7** illustrates this effect
for two TICs, hydrogen cyanide (HCN) and arsine (AsH_3) (7). To clarify the difference in analyte
pattern, the pattern due to air has been subtracted. Note that the patterns are not only readily
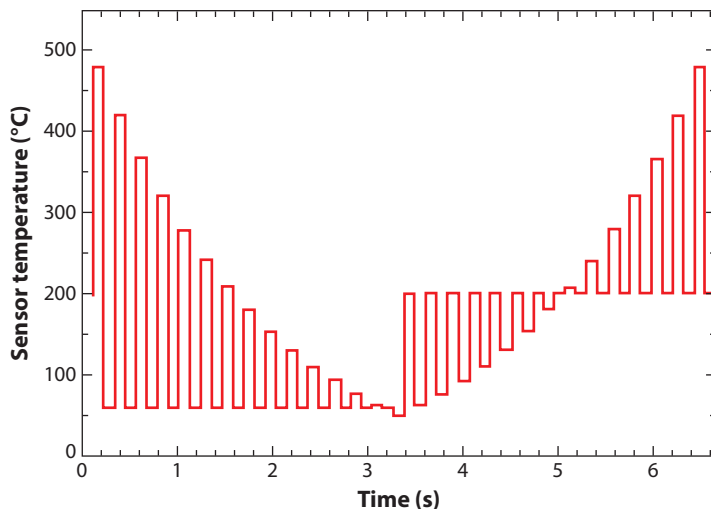distinguishable, but they are also repeatable from TPS cycle to cycle.

Figure 6

A typical temperature-programmed sensing program. In this example, film-conductance data can be collected at each sensor element 58 times in 6.5 seconds.
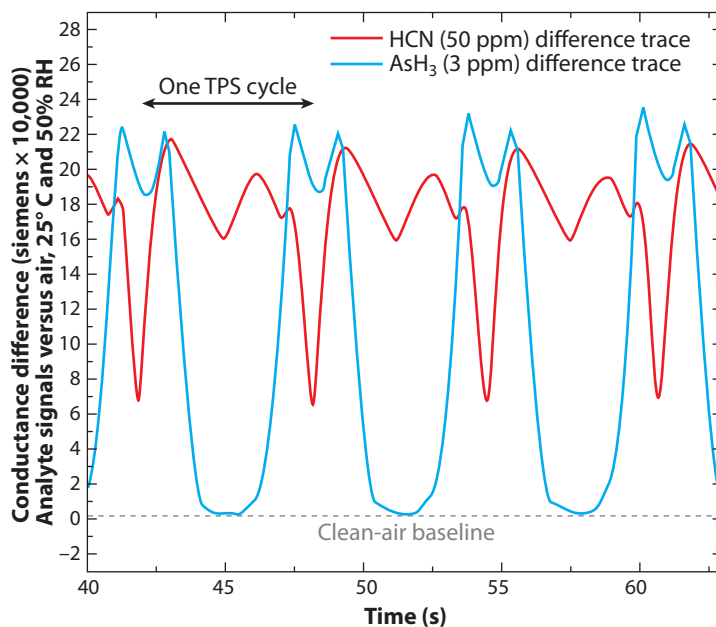

Figure 7

Comparison of temperature-programmed sensing traces for detection of arsine (AsH₃) and hydrogen cyanide (HCN) using the program shown in **Figure 6**. Difference traces highlight the component of the signal arising only from the analyte. Abbreviations: RH, relative humidity; TPS, temperature-programmed sensing.

3. INFORMATION EXTRACTION

A more sophisticated approach for dealing with data sets for problems of greater complexity than those presented in **Figure 7** is through application of pattern recognition methods. Statistical techniques (summarized in **Figure 8**) have been used extensively for handling generic pattern recognition tasks such as dimensionality reduction, classification, and clustering (29, 30).

We applied Fisher's linear discriminant analysis (LDA) (31) to the problem of visualizing chemical fingerprints from complex 2-D data sets (i.e., multiple materials and temperatures). Our
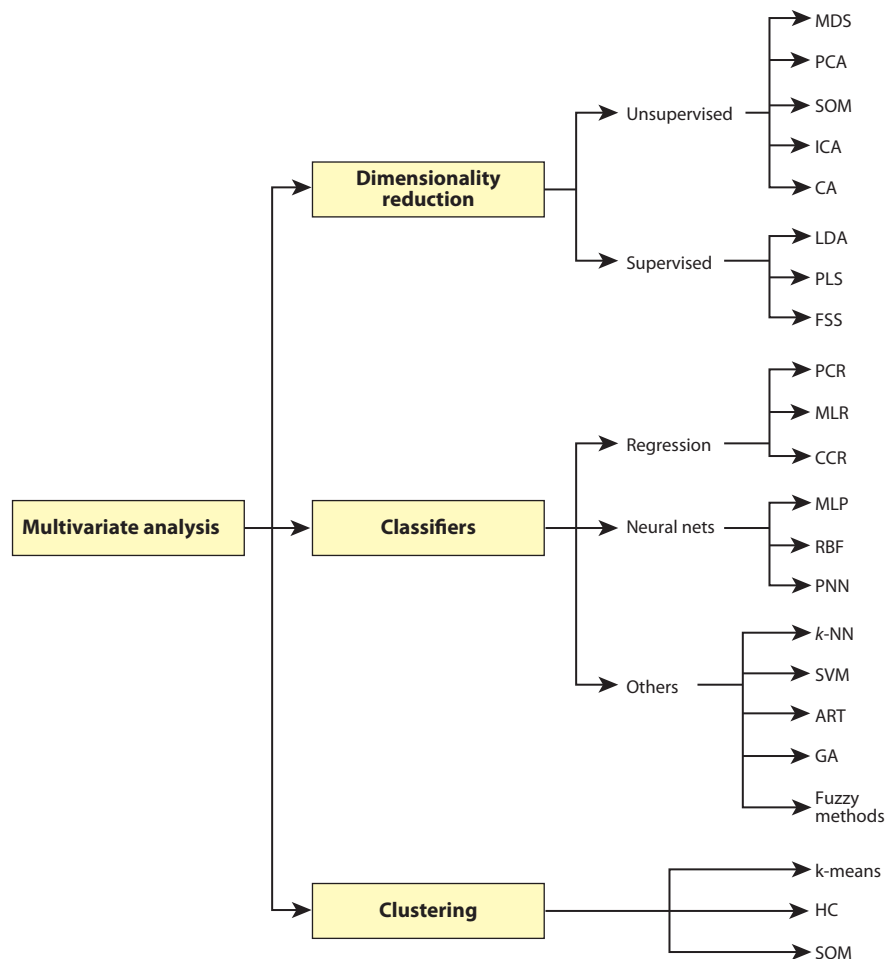

Figure 8

Statistical methods for multivariate pattern analysis techniques applied with gas sensor arrays (see References 29 and 30 for a review of these methods). Abbreviations: MDS, multidimensional scaling; PCA, principal component analysis; SOM, self-organized maps; ICA, independent component analysis; CA, cluster analysis; LDA, Fisher's linear discriminant analysis; PLS, partial least squares; FSS, feature selection search; PCR, principal component regression; MLR, multilinear regression; CCR, canonical correlation regression; MLP, multilayer perceptron; RBF, radial basis function; PNN, probabilistic neural network, k-NN, k–nearest neighbors; SVM, support vector machines; ART, adaptive resonance theory; GA, genetic algorithms; HC, hierarchical clustering.

analysis helped us determine whether the sensor measurements had enough information to solve a given analytical problem.

3.1. Detection of Single Targets: A One-Dimensional Approach

First, we considered a single chemical hazard, i.e., HCN, in the presence of different common interferences. To generate the analytical information required to solve this type of problem, responses from a single SnO_2 film that was cycled through 32 different temperatures (**Figure 6**) were analyzed. **Figure 9** (32) shows the scatter plot of the SnO_2 responses obtained by concatenating the conductance values of the sensing films at different temperatures and projecting them onto the first three LDA axes (maximizing separation between different conditions and simultaneously grouping responses to similar conditions). Because the data are truly distinguishable, a clear boundary exists between the states of analyte presence and absence. All of the states with HCN present, regardless of background, cluster at the upper right of the graph, whereas the safe conditions coalesce to the lower left, suggesting that this 1-D approach was sufficient to deal with this problem.

Rarely are problems in the real world this simple, however. Finding the solution to challenges involving a large variety of target analytes and background conditions requires a multidimensional approach. Other researchers have applied multidimensional data analysis solutions to data generated by bundled fiberoptic sensors (33), composite polymer sensors (34, 35), and colorimetric dye detectors (36, 37). In this review, we focus upon multidimensional analysis of databases generated
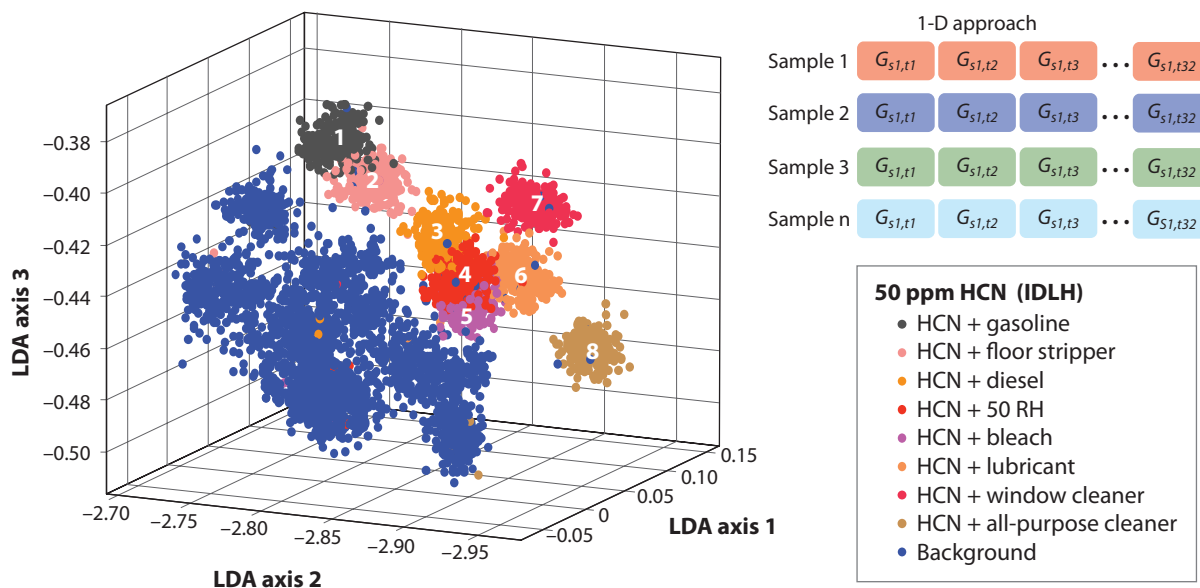

Figure 9

Linear discriminant analysis (LDA) for hydrogen cyanide (HCN) discrimination from a variety of backgrounds containing a range of interfering species. Color codes identify the analyte to which the sensor array was exposed when the measurements were made. Here, the response of a single SnO_2 sensor at multiple temperatures, i.e., a one-dimensional (1-D) approach, is used to distinguish different conditions. This dimensionality reduction analysis allows qualitative determination of the sufficiency of analytical information for the chosen task. A classification analysis would be required to demonstrate these results quantitatively. 1, HCN plus gasoline, 2, HCN plus floor stripper, 3, HCN plus diesel, 4, HCN plus 50 RH, 5, HCN plus bleach, 6, HCN plus lubricant, 7, HCN plus window cleaner, 8, HCN plus all-purpose cleaner. Abbreviations: IDLH, immediate danger to life and health; RH, relative humidity.

Annual Review of Analytical Chemistry 2009.2:463-484. Downloaded from www.annualreviews.org by Fordham University on 12/16/11. For personal use only.

www.annualreviews.org • Temperature-Programmed Microsensors   473

using conductometric metal oxide microsensor-array devices, which feature axes of both materials chemistry and temperature effects within their available data space.

3.2. Detection of Multiple Targets: A Two-Dimensional Approach

An example of a more complex problem involves the detection of five different targets: ammonia (NH), hydrogen cyanide (HCN), chlorine (CL), ethylene oxide (EO), and cyanogen chloride (CK) in different ambient and background conditions (**Figure 1**). To solve this problem, we began with a simple 1-D approach and examined four proposed 1-D solutions (**Figure 10**): (*a*) SnO_2, (*b*) SnO_2/TiO_2, (*c*) TiO_2, and (*d*) TiO_2/RuO_x, all operated using the same 32-step temperature program (32). Each data point indicates one of the six possible conditions of interest: presence of NH, HCN, CL, EO, CK, and any of the tested backgrounds without hazards. Each condition, in turn, could belong to any one of the several subconditions shown in **Figure 1**; for example, NH-positive samples could include all sensor responses to NH, with or without the four different interferences, at all three humidity conditions. None of the 1-D approaches can provide sufficient analytical information to solve this multianalyte problem.

We then systematically combined information from multiple films in a 2-D approach. **Figure 11** (32) illustrates how, when information from multiple films was combined, the separability of the target cluster from the background improved. When two copies of each sensing film are queried, distinguishable clusters of each of the five analytes separate from the central group of safe conditions. **Table 1** provides a quantitative summary of offline detection performance using this approach.

4. PRACTICAL OPERATION

4.1. Drift Correction

Before a sensor can be used to detect an analyte, it must first be "trained" on that analyte to extract chemical fingerprints for later comparison. Drift in sensor response over time can alter the chemical signatures; drift therefore represents a critical hurdle that must be overcome in order to achieve (near-)real-time recognition based on pretrained algorithms. **Figure 12*a*** presents a scatter plot of training samples and test samples collected weeks after training; for clarity, dimensionality reduction using principal component analysis (PCA) is employed. The test measurements reveal a relative spatial distribution of samples with and without HCN similar to that of the training data sets. However, the test samples are translated in PCA space away from the training samples by a magnitude exceeding the size of the original distribution. A careful analysis of signal baseline (response to air at 30% relative humidity) over these operating periods indicates that this translation is mainly due to changes in the sensor's baseline response over time. Moreover, initial-state offset contributions arising from extrasensory factors (e.g., power supply or electronic contact variation) cannot be discounted.

To compensate for sensor baseline changes, we investigated the following approach. In a constant background, the sensor response is relatively stable (i.e., there is a smaller derivative), whereas introducing a new analyte greatly changes the sensor response (i.e., there is a larger derivative). Therefore, the derivative of a sensor response over time can be used to track and constantly update the sensor baseline. Recomputing the subsequent sensor responses with respect to the most recently confirmed baseline response effectively removes the contribution of the baseline drift. The algorithm used to perform baseline correction is a continuous remapping function that depends upon generally observed properties of the baseline condition. **Figure 12*b*** shows the scatter plot
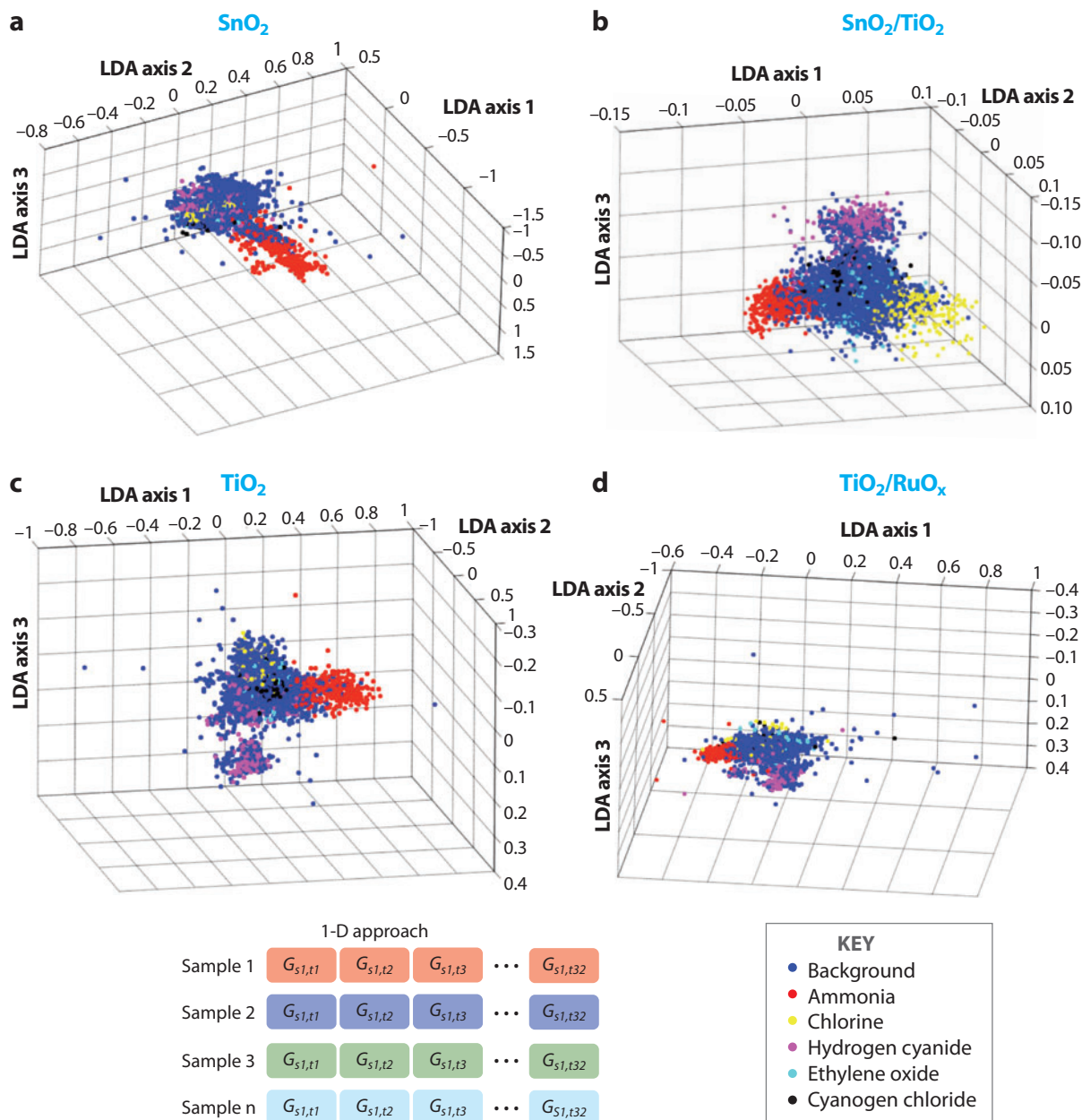
a SnO$_2$

b SnO$_2$/TiO$_2$

c TiO$_2$

d TiO$_2$/RuO$_x$

1-D approach

Sample 1	$G_{s1,t1}$	$G_{s1,t2}$	$G_{s1,t3}$	$\cdots$	$G_{s1,t32}$
Sample 2	$G_{s1,t1}$	$G_{s1,t2}$	$G_{s1,t3}$	$\cdots$	$G_{s1,t32}$
Sample 3	$G_{s1,t1}$	$G_{s1,t2}$	$G_{s1,t3}$	$\cdots$	$G_{s1,t32}$
Sample n	$G_{s1,t1}$	$G_{s1,t2}$	$G_{s1,t3}$	$\cdots$	$G_{s1,t32}$

KEY
- Background
- Ammonia
- Chlorine
- Hydrogen cyanide
- Ethylene oxide
- Cyanogen chloride

Figure 10

Scatter plots of the conductometric responses from (*a*) tin oxide (SnO$_2$), (*b*) SnO$_2$ and titanium oxide (TiO$_2$), (*c*) TiO$_2$, and (*d*) TiO$_2$ and ruthenium oxide (RuO$_x$) sensors at 32 different temperatures after dimensionality reduction using Fischer's linear discriminant analyses (LDAs). Each sensor was exposed to five targets under the conditions and delivery program identified in **Figure 1** at IDLH (immediate danger to life and health) concentrations and at three humidity levels (10%, 30%, or 70% RH) or included with the vapors (1% of dry air saturation) of glass cleaner, floor stripper, chlorine bleach, or all-purpose cleaners. This one-dimensional (1-D) approach did not yield a solution to the problem.
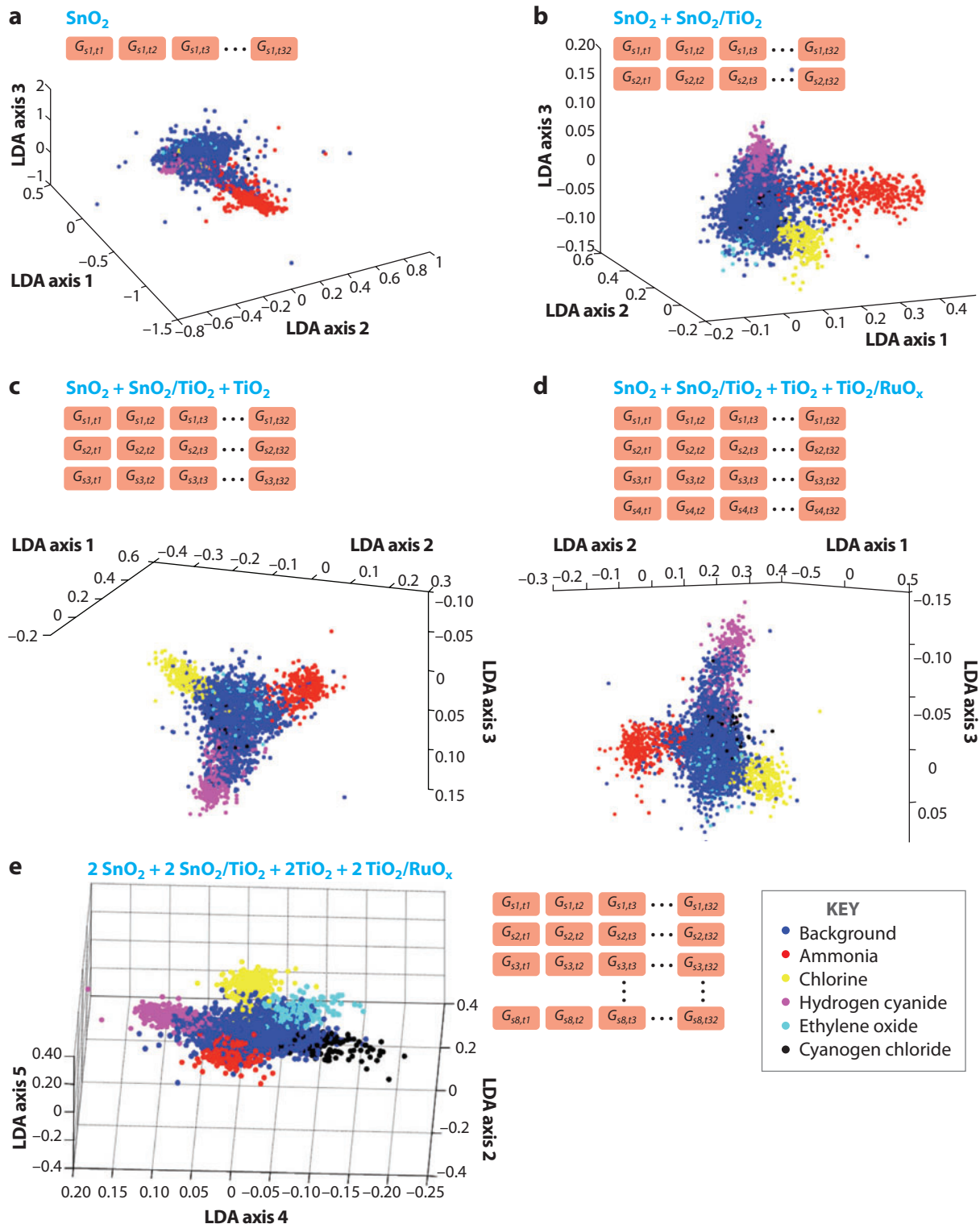
a SnO_2

$G_{s1,t1}$ $G_{s1,t2}$ $G_{s1,t3}$ $\cdots$ $G_{s1,t32}$

LDA axis 3

LDA axis 1

LDA axis 2

b $SnO_2 + SnO_2/TiO_2$

$G_{s1,t1}$ $G_{s1,t2}$ $G_{s1,t3}$ $\cdots$ $G_{s1,t32}$
$G_{s2,t1}$ $G_{s2,t2}$ $G_{s2,t3}$ $\cdots$ $G_{s2,t32}$

LDA axis 3

LDA axis 2

LDA axis 1

c $SnO_2 + SnO_2/TiO_2 + TiO_2$

$G_{s1,t1}$ $G_{s1,t2}$ $G_{s1,t3}$ $\cdots$ $G_{s1,t32}$
$G_{s2,t1}$ $G_{s2,t2}$ $G_{s2,t3}$ $\cdots$ $G_{s2,t32}$
$G_{s3,t1}$ $G_{s3,t2}$ $G_{s3,t3}$ $\cdots$ $G_{s3,t32}$

LDA axis 1

LDA axis 2

LDA axis 3

d $SnO_2 + SnO_2/TiO_2 + TiO_2 + TiO_2/RuO_x$

$G_{s1,t1}$ $G_{s1,t2}$ $G_{s1,t3}$ $\cdots$ $G_{s1,t32}$
$G_{s2,t1}$ $G_{s2,t2}$ $G_{s2,t3}$ $\cdots$ $G_{s2,t32}$
$G_{s3,t1}$ $G_{s3,t2}$ $G_{s3,t3}$ $\cdots$ $G_{s3,t32}$
$G_{s4,t1}$ $G_{s4,t2}$ $G_{s4,t3}$ $\cdots$ $G_{s4,t32}$

LDA axis 2

LDA axis 1

LDA axis 3

e $2 SnO_2 + 2 SnO_2/TiO_2 + 2TiO_2 + 2 TiO_2/RuO_x$

$G_{s1,t1}$ $G_{s1,t2}$ $G_{s1,t3}$ $\cdots$ $G_{s1,t32}$
$G_{s2,t1}$ $G_{s2,t2}$ $G_{s2,t3}$ $\cdots$ $G_{s2,t32}$
$G_{s3,t1}$ $G_{s3,t2}$ $G_{s3,t3}$ $\cdots$ $G_{s3,t32}$
$G_{s8,t1}$ $G_{s8,t2}$ $G_{s8,t3}$ $\cdots$ $G_{s8,t32}$

LDA axis 5

LDA axis 2

LDA axis 4

KEY
- ● Background
- ● Ammonia
- ● Chlorine
- ● Hydrogen cyanide
- ● Ethylene oxide
- ● Cyanogen chloride

Table 1   Microsensor recognition performance[a]

Analyte detected/ delivered[b]	Background (%)	NH (%)	HCN (%)	CL (%)	EO (%)	CK (%)
Background (%)	97.13	0.0065	0.0056	0.0084	0.0041	0.0041
NH (%)	0.0813	91.87	0	0	0	0
HCN (%)	0.1063	0	89.38	0	0	0
CL (%)	0.2366	0	0	76.34	0	0
EO (%)	0.1402	0	0	0	85.98	0
CK (%)	0.2977	0	0	0	0	70.23

[a]Performance is expressed as a percentage on a per-TPS (temperature-programmed sensing) cycle basis.

[b]All analytes were trained and tested with the analyte-delivery matrix shown in **Figure 1**. Abbreviations: CK, cyanogen chloride; CL, chlorine; EO, ethylene oxide; HCN, hydrogen cyanide; NH, ammonia.

of the remapped test responses to different conditions with and without HCN after this baseline correction. The test samples are now much closer to the training samples in PCA space (note the change in scale from **Figure 12*a*** to **Figure 12*b***).

4.2. Real-Time Detection

The best test of a sensor system is determining its ability to discriminate between analyte states unsupervised and in (near) real time. With the sensors' analytical capabilities visually and statistically confirmed, the training sequences complete, and the drift compensation algorithm in place, the system can be evaluated in an unsupervised detection mode. **Figure 13** shows the different analytes to which the sensor was exposed over time, the baseline-corrected response of two SnO_2 sensors at 32 different temperatures, and the performance of a *k*-nearest-neighbor classifier (31). When presented with the target/background exposure sequence from **Figure 1** roughly one month after the sensor array was trained, correct identification was made upon each presentation of NH_3 at the IDLH concentration (300 ppm). Although there was an apparent lag in the response, particularly upon recovery, all hazard-onset responses were recognized to within a few minutes of the hazard introduction.

5. FUTURE DIRECTIONS

Although the results discussed above represent key advances on several developmental fronts, a number of additional challenges must also be resolved before such sensor devices can be successfully used for early-warning applications. One such challenge is enabling a device to classify not-yet-known hazards. Another concerns transferring the trained coefficient set derived from data collected using a small group of devices to an entire manufacturing run. We have made progress on both of these points in proof of concept.

Figure 11

(*a–d*) A progression of scatter plots showing the effect on detection and discrimination performance for multiple targets in complex backgrounds as responses from different sensing materials are sequentially integrated into the plot. In this two-dimensional approach, the target clusters are more separable from the background cluster. Sufficient information for this problem is generated by combining information from two copies of the four sensors (*e*). Abbreviations: LDA, linear discriminant analysis; RuO_x, ruthenium oxide; SnO_2, tin oxide; TiO_2, titanium oxide.

a Before sensor baseline response removal

b After baseline response removal

Separate testing phase
+ HCN samples
• All background conditions
• Air samples at 30% RH

Training
+ HCN samples
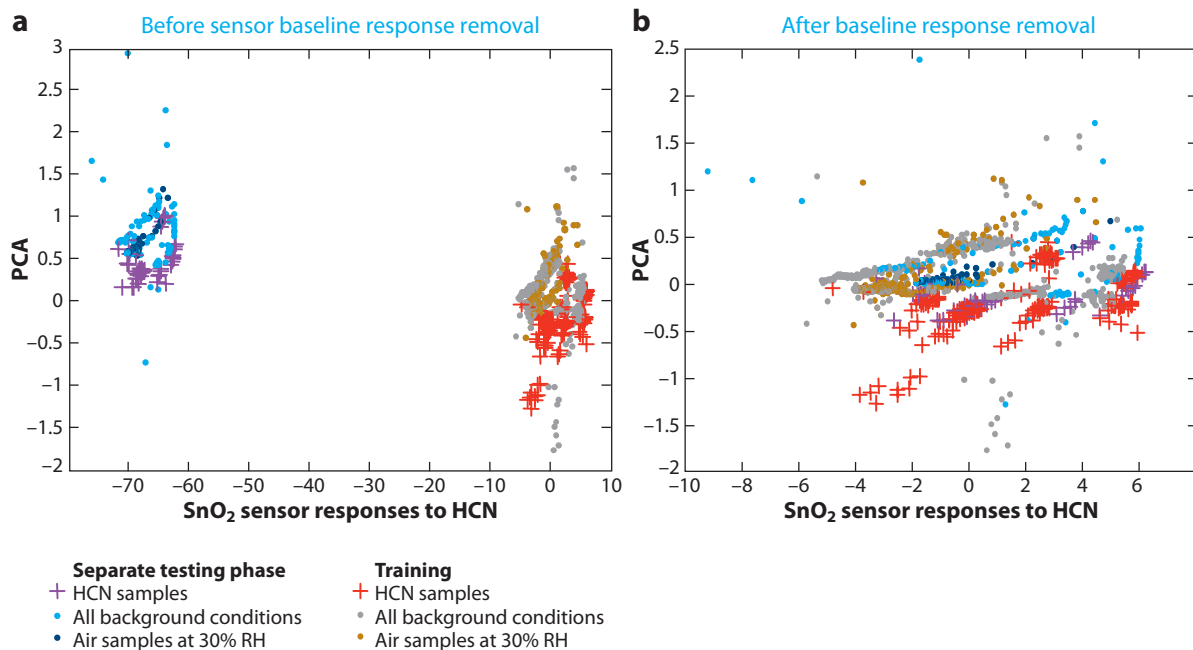• All background conditions
• Air samples at 30% RH

Figure 12

(*a*) Principal component analysis (PCA) showing scatter plots of tin oxide (SnO$_2$) sensor responses to hydrogen cyanide (HCN) in different background and humidity conditions during the training. Also shown are the results of a separate testing phase that followed training by one week. The test samples are translated in PCA space away from the training samples despite the similarity between the relative distributions of the measurements made in different conditions. (*b*) PCA plot after removing the contribution of sensor baseline response. Note the change in scale.

Analyte

30% RH
70% RH
10% RH
Floor stripper
Paint
Bleach
Window cleaner

SnO$_2$ sensors

k-NN   NH$_3$ present
prediction   NH$_3$ absent
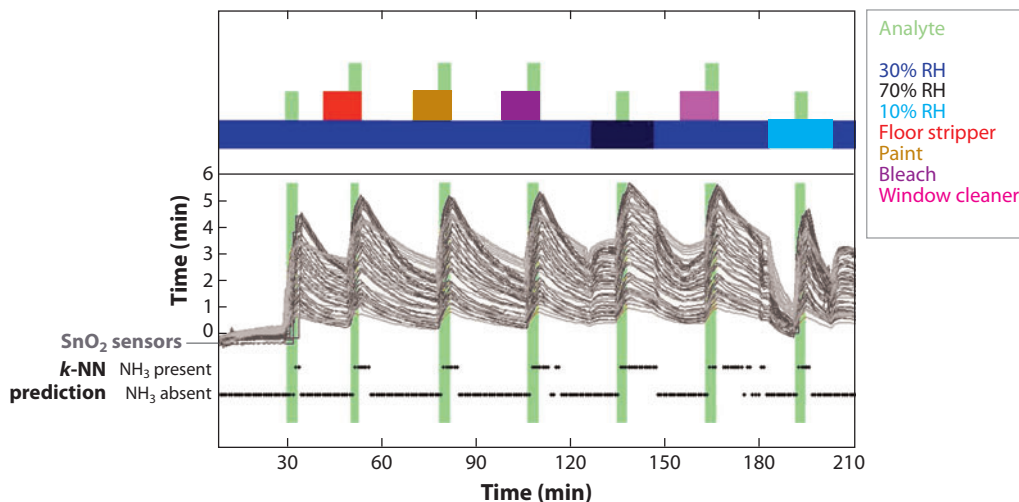
Figure 13

Real-time recognition of ammonia (NH$_3$) using a chemical-microsensor array one month posttraining. The different conditions are shown on top; 32 isotherms (measurements at a fixed temperature) of two tin oxide (SnO$_2$) sensors are shown in gray. Prediction of presence or absence of NH$_3$ (*two levels of* y *axis*) with a pretrained *k*-nearest-neighbor (*k*-NN) classifier is shown in black below the raw sensor responses. Despite the response lag, the combined system correctly identifies each NH$_3$ presentation.

5.1. Hierarchical Classification of Functional Groups

The sheer number of hazardous chemicals makes training for all known hazards prohibitive. Although they span a considerable range of molecular properties, the five analytes considered here do not cover the chemistries of many of the CWAs and TICs in use today. More sobering is the notion that a belligerent will develop or utilize a hazardous compound that we have not yet encountered or that has not previously been weaponized. Many hazardous compounds contain the same functional groups; for example, the nerve agents and a common class of pesticides are organic phosphonates (38, 39). Chemical reactions are characterized by the interactions between functional groups; it may be feasible to extract functional-group information from the temperature-dependent transduction features within our chemical-sensor-array databases. A proof-of-concept experiment has been completed using volatile organic chemicals as targets; the experimental results demonstrated that hierarchical analyte classification has merit (40). A schematic of this approach is shown in **Figure 14**. A series of algorithms operates at each step to extract (*a*) basic information ("Is the analyte background dry air, a simple oxide, or an organic compound?") and then (*b*) more specific information ("Does this oxygen-containing organic compound contain a hydroxyl/alcohol group
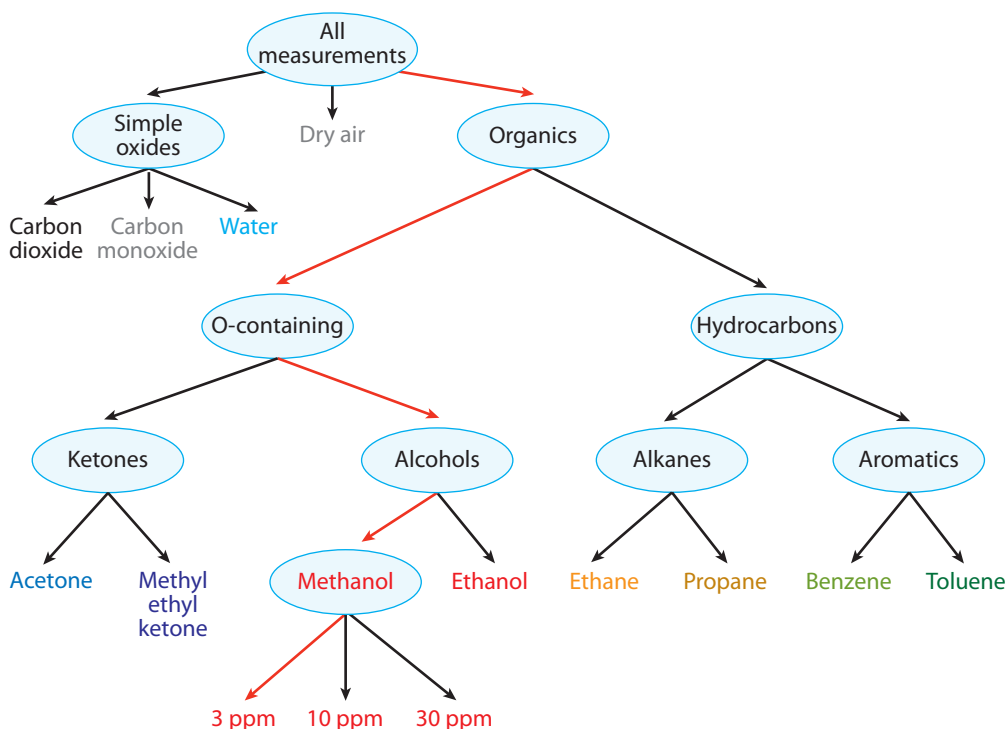
Figure 14

A schematic of hierarchical analyte identification by functional group. The base levels (*top*) deal with general characteristics that are shared among several analytes and hence that generalize to chemicals within the same chemical class. As we progress to more specific characteristics in the hierarchical tree (*center*), specific features unique to a subclass of analytes are added to refine the chemical identity. The most specific branches (*bottom*) deal with species recognition and quantification. At each stage, only sensor-response features that can best solve the specific task are used.
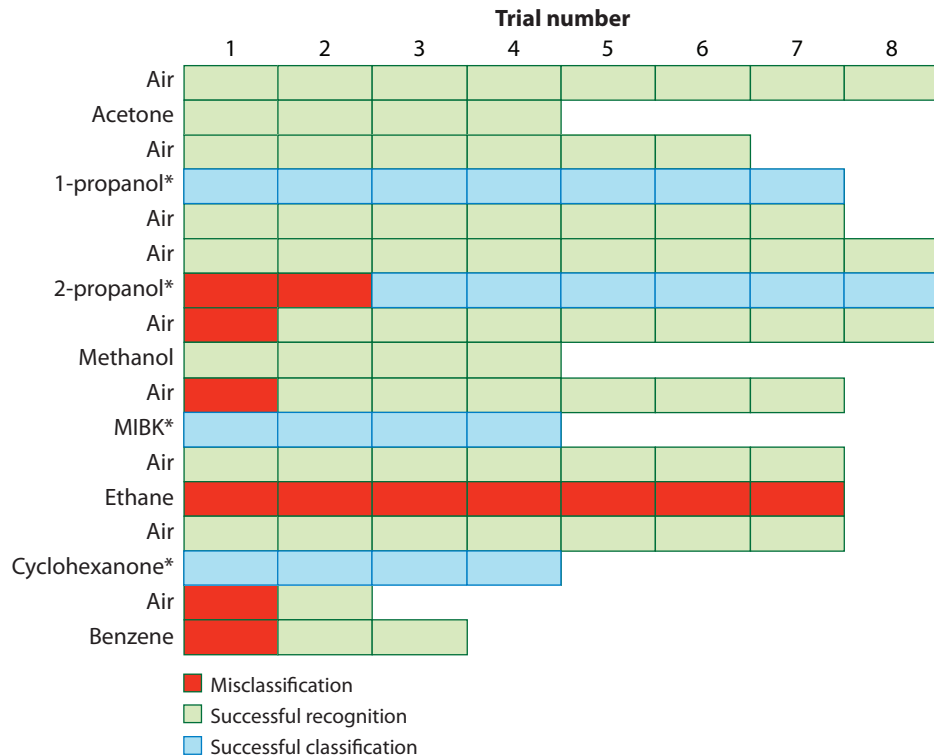
Figure 15

Preliminary results using the hierarchical discrimination algorithm to identify a number of tested volatile organic compounds as well as to classify a number of unknowns (denoted with asterisks) that were not presented during the training phase. Most compounds tested in the experiment were correctly recognized (*green*) or classified (*blue*). Misclassifications (*red*) occurred mostly during a transition measurement phase following introduction or removal of an analyte. Sensitivity to ethane was lost due to a deliberate aging process performed between the training and testing phases to study the robustness of this approach to response drift over time. Abbreviation: MIBK, methyl isobutyl ketone.

or a secondary carbonyl/ketone group?"). Eventually, enough information is selectively extracted at each step to identify the compound. Although the lower levels of the algorithm are specific and pertain to recognition of each trained analyte, the higher levels concern more generic problems and are more suitable for generalization (i.e., classification of compounds that are unknown but that belong to the same class or subclass). **Figure 15** presents the results of this approach from

Figure 16

(*a*) Cross-correlation plot of a single sensor element's response to ammonia (NH_3), in which the degree of data redundancy between two points in a temperature program is determined. Each pixel in the picture provides the correlation between responses of that sensor [in this case, titanium oxide (TiO_2)] at two different temperatures. Lighter squares denote higher correlations, i.e., redundant information, and darker squares denote uncorrelated data points. Generally, measurements made at high temperatures using the TiO_2 sensor are not correlated with those made at lower temperatures. (*b*) Correlation plot for NH_3 detection using two copies of each material film. The degree of similarity between correlation patterns of the same sensing-film type is a measure of their reproducibility. Whereas the films made up entirely of bulk oxides [tin oxide (SnO_2) and TiO_2] generated data that was largely reproducible from sensor to sensor, the films that included ruthenium-coated titanium dioxide (RuO_x/TiO_2) did not correlate well with each other, indicating that certain manufacturing challenges have yet to be overcome.

a sensor tested with both trained analytes and new analytes that share chemical features with the trained ones. With the exception of ethane, the diverse compounds in the study, both knowns (presented during training) and unknowns (presented only during testing), were recognized or classified correctly most of the time.

a

Ammonia recognition problem (TiO$_2$ film)

■ Indicates relatively low correlation between TiO$_2$ at 60° C versus TiO$_2$ at 460° C

□ Indicates high correlation between TiO$_2$ at 60° C versus TiO$_2$ at 131° C

High

Low

b

Replica 1   Replica 2

SnO$_2$ SnO$_2$/TiO$_2$ TiO$_2$ TiO$_2$/RuO$_x$ SnO$_2$ SnO$_2$/TiO$_2$ TiO$_2$ TiO$_2$/RuO$_x$

Replica 1
SnO$_2$
SnO$_2$/TiO$_2$
TiO$_2$
TiO$_2$/RuO$_x$

Replica 2
SnO$_2$
SnO$_2$/TiO$_2$
TiO$_2$
TiO$_2$/RuO$_x$

(Shown for NH$_3$)
Reproducible films: SnO$_2$, SnO$_2$/TiO$_2$, TiO$_2$

5.2. Manufacturability

It would be prohibitively costly in time and materials to individually train each sensor prior to deployment. The sensors are expected to have limited lifetimes, and ideally most of their lifetimes would be spent in the field taking measurements, not undergoing training. Furthermore, as the total trained database becomes more extensive, "boutique" packages of temperature programs and decision algorithms that most closely match the hazards more probable in a particular application space become more desirable. For instance, an agricultural product–manufacturing facility could be tuned for pesticides and ammonia, with a particular focus on hydrocarbon fuel interferences, whereas an office building's security could be better enhanced with training for warfare agents in the presence of cleaning products and perfumes. Thus, training sets should be valid for all sensors fabricated using a given procedure, which can be realized as long as fabrication reproducibility is within a given level of tolerance.

To evaluate the reproducibility of sensors, we propose a novel method based on correlation coefficients. For the NH-detection problem shown in **Figure 1** (all targets are NH_3), **Figure 16a** shows the pairwise correlation between TiO_2 responses at different temperatures. The greater the correlation between two isothermal responses of the same material, the more similar or redundant is the information generated. A more comprehensive correlation-analysis plot between two copies of each of the four materials is shown in **Figure 16b**. Replicas of the four sensing films used in this study underwent the same training program on the same device. To be considered reproducible, different copies of the same film should have essentially identical self- and cross-correlation patterns. As shown in **Figure 16**, SnO_2 and TiO_2/SnO_2 are highly reproducible. TiO_2, although less correlated, can still generate transferrable data. However, Ru/TiO_2 is not sufficiently reproducible to consider transferring training. Future studies focusing on reproducibility are needed to improve these films' property tolerances and similarity of performance.

6. CONCLUSIONS

Sensor-based detection of hazardous analytes in dynamic, real-world environments is a complex task. We have described a small, high-speed, versatile chemical-microsensor platform and have shown its ability to generate orthogonal data through materials selection and temperature programming. We have demonstrated that these temperature-programmed chemical microsensors can generate voluminous data sets; applying advanced data-reduction algorithms allows identification of analytes present in the system, thereby providing a promising solution to this complex problem. Visual inspection of data sets reveals device selectivity, but statistical analyses are required for more sophisticated tasks. We have addressed the practical considerations surrounding long-term deployment, specifically the identification and correction of signal drift and the challenges surrounding real-time, unsupervised operation. Additional advances for both devices and signal-processing algorithms, including repeatable device manufacturability and hierarchical classification (wherein previously untested analyte species can be classified by identifiable interactions of their functional groups) show considerable promise.

Note that the data-reduction approaches discussed here are not limited to responses generated by NIST microsensors; in fact, we speculate that integrating data contributions of other devices known to possess viable analytical capabilities in this field, such as cermet sensors (41), capacitive microsensors (42), and surface acoustic wave devices (43, 44), will result in instruments ranging from the 2-D data generator discussed above to 3-D and higher database dimensionality. Such sensors will improve selectivity and thereby reduce false positives—a very important detector confidence factor.

DISCLOSURE STATEMENT

ACKNOWLEDGMENTS

LITERATURE CITED

1. Hierlemann A, Gutierrez-Osuna R. 2008. Higher-order chemical sensing. *Chem. Rev.* 108:563–613
2. Cavicchi RE, Semancik S, DiMeo F, Taylor CJ. 2003. Use of microhotplates in the controlled growth and characterization of metal oxides for chemical sensing. *J. Electroceram.* 9:155–64
3. Semancik S, Cavicchi RE, Wheeler MC, Tiffany JE, Poirier GE, et al. 2001. Microhotplate platforms for chemical sensor research. *Sens. Actuators B* 77:579–91
4. Semancik S, Cavicchi RE, Gaitan M, Suehle JS. 1994. *U.S. Patent No. 5,345,213*
5. Taylor CJ, Semancik S. 2002. Use of microhotplate arrays as microdeposition substrates for materials exploration. *Chem. Mater.* 14:1671–77
6. Benkstein KD, Martinez CJ, Li G, Meier DC, Montgomery CB, Semancik S. 2006. Integration of nanostructured materials with MEMS microhotplate platforms to enhance chemical sensor performance. *J. Nanopart. Res.* 8:809–22
7. Meier DC, Evju JK, Boger Z, Raman B, Benkstein KD, et al. 2007. The potential for and challenges of detecting chemical hazards with temperature-programmed microsensors. *Sens. Actuators B* 121:282–94
8. Taylor CJ, Gilmer DC, Colombo DG, Wilk GD, Campbell SA, et al. 1999. Does chemistry really matter in the chemical vapor deposition of titanium dioxide? Precursor and kinetic effects on the microstructure of polycrystalline films. *J. Am. Chem. Soc.* 121:5220–29
9. Taguchi N. 1972. *U.S. Patent No. 3,695,848*
10. Martinez CJ, Hockey B, Montgomery CB, Semancik S. 2005. Porous tin oxide nanostructured microspheres for sensor applications. *Langmuir* 21:7937–44
11. Li G, Martinez C, Semancik S, Smith JA, Josowicz M, Janata J. 2004. Effect of morphology on the response of polyaniline-based conductometric gas sensors: nanofibers versus thin films. *Electrochem. Solid State Lett.* 7:H44–47
12. Ryan MA, Zhou HY, Buehler MG, Manatt KS, Mowrey VS, et al. 2004. Monitoring space shuttle air quality using the Jet Propulsion Laboratory electronic nose. *IEEE Sens. J.* 4:337–47
13. Panchapakesan B, Devoe DL, Widmaier MR, Cavicchi R, Semancik S. 2001. Nanoparticle engineering and control of tin oxide microstructures for chemical microsensor applications. *Nanotechnology* 12:336–49
14. Meier DC, Semancik S, Button B, Strelcov E, Kolmakov A. 2007. Coupling nanowire chemiresistors with MEMS microhotplate gas sensing platforms. *Appl. Phys. Lett.* 91:063118
15. Wheeler MC, Tiffany JE, Walton RM, Cavicchi RE, Semancik S. 2001. Chemical crosstalk between heated gas microsensor elements operating in close proximity. *Sens. Actuators B* 77:167–76
16. Meier DC, Taylor CJ, Cavicchi RE, White VE, Semancik S, et al. 2005. Chemical warfare agent detection using MEMS-compatible microsensor arrays. *IEEE Sens. J.* 5:712–25
17. Vermont Safety Resources, Inc. 2006. *Chemical identification: phosphonofluoridic acid, methyl-, isopropyl ester.* **http://hazard.com/msds/tox/tf/q96/q884.html**. Last accessed 7 Oct. 2008
18. Boger Z, Meier DC, Cavicchi RE, Semancik S. 2003. Rapid identification of chemical warfare agents by artificial neural network pruning of temperature-programmed microsensor databases. *Sens. Lett.* 1:86–92

19. Cavicchi RE, Walton RM, Aquino-Class M, Allen JD, Panchapakesan B. 2001. Spin-on nanoparticle tin oxide for microhotplate gas sensors. *Sens. Actuators B* 77:145–54

20. Iftimie N, Luca D, Lacomi F, Girtan M, Mardare D. 2009. Gas sensing materials based on TiO_2 thin films. *J. Vac. Sci. Technol. B*. 27:538–41

21. Arshak K, Gaidan I. 2005. Development of a novel gas sensor based on oxide thick films. *Mat. Sci. Eng. B: Solid State Mat. Adv. Technol.* 118:44–49

22. Goschnick J, Haeringer D, Kiselev I. 2007. Multicomponent quantification with a novel method applied to gradient gas sensor microarray signal patterns. *Sens. Actuators B* 127:237–41

23. Haeringer D, Goschnick J. 2008. Characterization of smelling contaminations on textiles using a gradient microarray as an electronic nose. *Sens. Actuators B* 132:644–49

24. Gutierrez-Osuna R, Gutierrez-Galvez A, Powar N. 2003. Transient response analysis for temperature-modulated chemoresistors. *Sens. Actuators B* 93:57–66

25. Nakata S, Okunishi H, Nakashima Y. 2006. Distinction of gases with a semiconductor sensor under a cyclic temperature modulation with second-harmonic heating. *Sens. Actuators B* 119:556–61

26. Vergara A, Ramirez JL, Llobet E. 2008. Reducing power consumption via a discontinuous operation of temperature-modulated micro-hotplate gas sensors: application to the logistics chain of fruit. *Sens. Actuators B* 129:311–18

27. Cavicchi RE, Suehle JS, Kreider KG, Gaitan M, Chaparala P. 1995. Fast temperature-programmed sensing for microhotplate gas sensors. *IEEE Electron Device Lett.* 16:286–88

28. Kunt TA, McAvoy TJ, Cavicchi RE, Semancik S. 1998. Optimization of temperature programmed sensing for gas identification using microhotplate sensors. *Sens. Actuators B* 53:24–43

29. Pearce TC. 1997. Computational parallels between the biological olfactory pathway and its analogue 'the electronic nose'. Part II. Sensor-based machine olfaction. *BioSystems* 41:69–90

30. Gutierrez-Osuna R. 2002. Pattern analysis for machine olfaction: a review. *IEEE Sens. J.* 3:189–202

31. Duda RO, Hart PE, Stork DG. 2001. Maximum-likelihood and Bayesian parameter estimation. In *Pattern Classification*, ed. RO Duda, PE Hart, DG Stork, pp. 117–21. New York: Wiley. 654 pp.

32. Raman B, Meier DC, Evju JK, Semancik S. 2009. Designing and optimizing microsensor arrays for recognizing chemical hazards in complex environments. *Sens. Actuators B*. In press

33. Gorris HH, Blicharz TM, Walt DR. 2007. Optical-fiber bundles. *FEBS J.* 274:5462–70

34. Woodka MD, Brunschweig BS, Lewis NS. 2007. Use of spatiotemporal response information from sorption-based sensor arrays to identify and quantify the composition of analyte mixtures. *Langmuir* 23:13232–41

35. Pardo M, Sisk BC, Sberveglieri G, Lewis NS. 2006. Comparison of Fisher's linear discriminant to multi-layer perceptron networks in the classification of vapors using sensor array data. *Sens. Actuators B* 115:647–55

36. Suslick KS, Rakow NA, Sen A. 2004. Colorimetric sensor arrays for molecular recognition. *Tetrahedron* 60:11133–38

37. Bang JH, Lim SH, Park E, Suslick KS. 2008. Chemically responsive nanoporous pigments: colorimetric sensor arrays and the identification of aliphatic amines. *Langmuir* 24:13168–72

38. Liu G, Lin Y. 2005. Electrochemical sensor for organophosphate pesticides and nerve agents using zirconia nanoparticles as selective sorbents. *Anal. Chem.* 77:5894–901

39. Hill HH, Martin SJ. 2002. Conventional analytical methods for chemical warfare agents. *Pure Appl. Chem.* 74:2281–91

40. Raman B, Hertz JL, Benkstein KD, Semancik S. 2008. A hierarchical methodology for odor recognition using chemical sensor arrays. *Anal. Chem.* 80:8364–71

41. Hammond MH, Johnson KJ, Rose-Pehrsson SL, Ziegler J, Walker H, et al. 2006. A novel chemical detector using cermet sensors and pattern recognition methods for toxic industrial chemicals. *Sens. Actuators B* 116:135–44

42. Mlsna TE, Cemalovic S, Warburton M, Hobson ST, Mlsna DA, Patel SV. 2006. Chemicapacitive microsensors for chemical warfare agent detection and toxic industrial chemical detection. *Sens. Actuators B* 116:192–201

43. Seto Y, Kanamori-Kataoka M, Tsuge K, Ohsawa I, Matsushita K, et al. 2005. Sensing technology for chemical-warfare agents and its evaluation using authentic agents. *Sens. Actuators B* 108:193–97

44. Harris CM. 2003. Seeing SAW potential. *Anal. Chem.* 75:355–58A

**Annual Review of
Analytical Chemistry**

Volume 2, 2009

Contents

Errata

An online log of corrections to *Annual Review of Analytical Chemistry* articles may be found at http://anchem.annualreviews.org/errata.shtml